Experimental versus computational determination of the dynamical model of a glider

Ana Carolina DOS SANTOS PAULINO *⋆,⋄, Antoine MURIE⋆,⋄, Thomas PAVOT⋄, Martin LEFEBVRE⋆,⋄, Renaud KIEFER⋆,⋄, Edouard LAROCHE⋆, Sylvain DURAND⋆,⋄
⋆ICube Laboratory (UMR CNRS 7357), Strasbourg university, Strasbourg, France.
⋄ Institut National des Sciences Appliquées (INSA), Strasbourg, France.

ABSTRACT

In this paper we present and compare two aircraft model identification techniques that are easy to implement and suitable for various airplane models, gliders comprised. One of them relies on flight data, while the second one uses a virtual model of the plane. To obtain the flight data, we propose a flight protocol that is simple to follow. Our analysis show that the methods find resembling results for similar airspeeds.

1 INTRODUCTION

Autonomous flight of aircraft is a subject that has drawn attention of both academia and companies since many years [1]. Several laboratories in this field, such as ETH Zurich's Autonomous Systems Lab, the Drone Lab in Hohschule Rhein-Wall, and the Uninhabited Aerial Vehicle Lab in the University of Minnesota, as well as companies, such as Parrot, DJI and Xiaomi, are investing in research and development of new models as this market is promising for the years to come. As a matter of fact, estimatives of commercial drone revenues indicate a growth from US$1 billion in 2018 to around US$12.6 billion in 2025[1]. The range of applications in logistics, surveillance, security and entertainment is vast and promising, stimulating the development of solutions both in hardware and in software.

In order to autonomously control an Unmanned Aerial Vehicle (UAV), it is useful to design a dynamic model that reproduces its input-output behavior. Such a model might enable the realization of a stability analysis and, later, the implementation of a model-based control strategy. The choice of a dynamical model takes into account the trade-off between the simplicity of the model and its precision over the entirety of the operation point envelope. We seek a model that represents the real aircraft as close as possible into the operation conditions with affordable complexity. Research of the numerical coefficients of the dynamical model that will lead to a reasonable representation of reality is named as *model identification*. It can be done with in-flight and off-flight data [2, 3], and may count on CAD-type softwares (XFLR5, CREO, StarCCM+).

To the best of the authors' knowledge, in the myriad of works about aircraft model identification available, surveys on different flight protocols for identification are not prolific, so that the beginners in the field have little information on which are the suitable signals to excite the dynamical system. Besides, in the universe of modeling and control of aircraft, few comparisons between different identification methods are performed for fixed wing. Among the found techniques, some require expensive setup or firmware modifications [4, 5]. Therefore, the contributions we aim to provide through this paper are the following: first, an overview on the different identification techniques found in the literature is provided; second, two different strategies for the identification of the dynamic model of an aircraft are proposed; and third, a simple flight protocol that provides relevant data for in-flight identification is established. The aforementioned identification strategies are convenient for various types of aircrafts: one of them uses in-flight data that is processed with well-known system identification numerical tools, and the other uses a numerical model for the aerodynamic coefficients' computation. We show that, for the identification of the relationship between aileron deflection and roll angle, both techniques lead to models that are close to each other when subject to the same airspeed.

The present article has the given structure: section 2 describes the setup used in our study, section 3 details the proposed identification techniques and conveys the numerical results found, and in section 4, we conclude this manuscript and evoke some perspectives on future work.

2 TEST SETUP

In this study, the choice was made to use a commercially available remote-controlled aircraft, i.e. an *Epsilon* glider[2], with a standard aircraft geometry. This airplane has many advantages: it is easy to handle, allows gliding and is inexpensive. It has two ailerons, two flaps, one elevator, one rudder and a thruster. Its dimensions make it easy to implement a flight controller in order to transform this aircraft into a drone and recover all flight data. The relative speed of the aircraft is a fundamental information for model characterization, being used in aicraft standard control laws. For these reasons, a Pitot probe was installed on the plane. This probe is the only

*Email address: ac.dossantos@unistra.fr

[1] https://www.tractica.com/newsroom/press-releases/commercial-drone-hardware-and-services-revenue-to-reach-12-6-billion-by-2025/

[2] https://www.absolu-modelisme.com/epsilon-competition-v3-pnp.html

addition to the original structure of the Epsilon glider. Some data from our glider in flight can be found in Table 1.

Wingspan	3.5 m	**Chord**	20.4 cm
Mass	3098 g	**Aspect ratio**	20.47
Length	1.5 m	**Speed**	10-25 m/s
Airfoil	MH32	**Battery**	LiPo 4S 1400 mAh

Table 1: Glider specifications.

To control our Epsilon glider, we use a Pixhawk board. It is an independent open-hardware project which supports multiple open source flight stacks such as PX4 and ArduPilot. The Pixhawk board has several advantages: its accessibility, its low cost and its very active community (scientific and industrial). In the case of this study we chose to work with PX4 because its code allows a great adaptability of the geometries. Through a *mixer file*, it is possible to develop a custom firmware that associates each actuator with a movement (roll, pitch and yaw)[3]. The Epsilon glider uses 7 of the 14 PWM outputs available on the Pixhawk board to operate the entire drone. A more detailed explanation of the positive and negative aspects of using PX4 and several other types of firmware has been done in [6].

3 AIRCRAFT MODEL IDENTIFICATION

In the first part of our study, we are interested in modeling the input-output relationship of our aircraft through a linear dynamic model. We take as control inputs the control surfaces: aileron, elevator and rudder; and as outputs, the plane attitude angles: roll, pitch and yaw. The relations between control surface inputs and plane angular displacements in each axis is modeled by transfer functions, and we assume that the dynamics for each axis are decoupled. This means that control surfaces aileron, elevator and rudder influence respectively roll, pitch and yaw angles. However, in practice, the use of one control surface has an influence over other axes so that, for example, the ailerons produce a yawing moment in addition to a rolling moment when they are deflected [7]. As a matter of fact, vertical and horizontal stabilizers on the tail of the plane and differential mixers on flaps tend to reduce this effect.

3.1 Model structure

The mathematical modeling of an aircraft has been detailed in several sources [1, 2, 3, 8, 9, 10] and can be obtained through Newton's law applied to translational and rotational movements. Here, we present the nonlinear model of a fixed wing plane that will be linearized around an operation point to obtain the aileron-roll transfer function. The mathematical notations summarized in Table 2 and represented in the aircraft body frame in Figure 1, are borrowed from [8].

[3] `https://dev.px4.io/en/`

p_n, p_e, p_d	positions north, east, down in inertial frame
u, v, w	velocities north, east, down in body frame
ϕ, θ, ψ	roll, pitch and yaw angles
p, q, r	roll, pitch and yaw rate angles in inertial frame
M	airplane mass
g	gravitational acceleration
S	wing area
b	wingspan
c	wing main chord
ρ	air density
f_x, f_y, f_z	forces north, east, down in body frame
l, m, n	roll, pitch and yaw moments in body frame
J_x, J_z	moments of inertia
J_{xz}	product of inertia
F_g^b	gravitational forces in body frame
V_a^b	airspeed in body frame
u_w, v_w, w_w	windspeeds in body frame
C_L, C_D, C_Y, C_l, C_m, C_n	nondimensional aerodynamic coefficients
$C_{l_{\delta_a}}$, $C_{n_{\delta_a}}$, C_{n_p}, C_{l_p}	aerodynamic coefficients
α, β	angle of attack and sideslip
δ_a, δ_e, δ_r	aileron, elevator and rudder angles

Table 2: Nomenclature table.

3.1.1 Kinematics

The expressions of the state variables relative to the ground with respect to the ones relative to the body of the plane are expressed in equations (1) and (2), where c_θ and s_θ stand for $\cos\theta$ and $\sin\theta$ respectively.

$$\begin{pmatrix} \dot{p_n} \\ \dot{p_e} \\ \dot{p_d} \end{pmatrix} = \begin{pmatrix} c_\phi c_\theta & c_\phi s_\theta s_\psi - s_\phi c_\psi & c_\phi s_\theta c_\psi + s_\phi s_\psi \\ s_\phi c_\theta & s_\phi s_\theta s_\psi + c_\phi c_\psi & s_\psi s_\theta c_\phi - c_\phi s_\psi \\ s_\theta & -c_\theta s_\psi & -c_\theta c_\psi \end{pmatrix} \begin{pmatrix} u \\ v \\ w \end{pmatrix} \tag{1}$$

$$\begin{pmatrix} \dot{\phi} \\ \dot{\theta} \\ \dot{\psi} \end{pmatrix} = \begin{pmatrix} 1 & \sin\phi\tan\theta & \cos\phi\tan\theta \\ 0 & \cos\phi & -\sin\phi \\ 0 & \frac{\sin\phi}{\cos\theta} & \frac{\cos\phi}{\cos\theta} \end{pmatrix} \begin{pmatrix} p \\ q \\ r \end{pmatrix} \tag{2}$$

3.1.2 Dynamic motion

By applying the second Newton's law, the translational and rotational dynamic motions can be expressed as in (3) and (4)

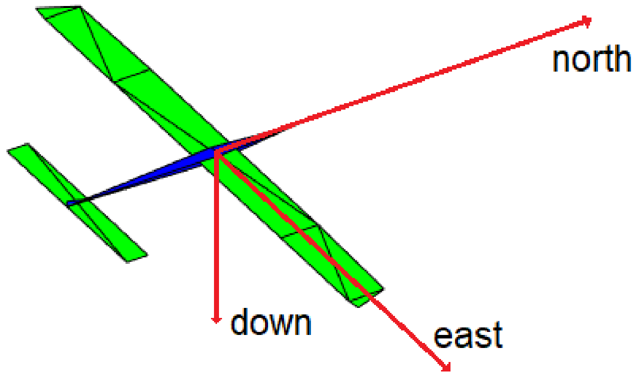

Figure 1: Aircraft with body axes north (roll axis), east (pitch axis) and down (yaw axis).

respectively:

$$\begin{pmatrix} \dot{u} \\ \dot{v} \\ \dot{w} \end{pmatrix} = \begin{pmatrix} rv - qw \\ pw - ru \\ qu - pv \end{pmatrix} + \frac{1}{M}\begin{pmatrix} f_x \\ f_y \\ f_z \end{pmatrix} \tag{3}$$

$$\begin{pmatrix} \dot{p} \\ \dot{q} \\ \dot{r} \end{pmatrix} = \begin{pmatrix} \Gamma_1 pq - \Gamma_2 qr + \Gamma_3 l + \Gamma_4 n \\ \Gamma_5 pr - \Gamma_6 \left(p^2 - r^2\right) + \Gamma_7 m \\ \Gamma_8 pq - \Gamma_1 qr + \Gamma_4 l + \Gamma_9 n \end{pmatrix} \tag{4}$$

with

$$\begin{cases} l = \frac{1}{2}\rho V_a^2 SbC_l(\beta, p, r, \delta_a, \delta_r) \\ m = \frac{1}{2}\rho V_a^2 ScC_m(\alpha, q, \delta_e) \\ n = \frac{1}{2}\rho V_a^2 SbC_n(\beta, p, r, \delta_a, \delta_r) \end{cases} \tag{5}$$

and

$$\begin{cases} \Gamma_1 = \frac{J_{xz}\left(J_x - J_y + J_z\right)}{\Gamma} & \Gamma_6 = \frac{J_{xz}}{J_y} \\ \Gamma_2 = \frac{J_z\left(J_z - J_y\right) + J_{xz}^2}{\Gamma} & \Gamma_7 = \frac{1}{J_y} \\ \Gamma_3 = \frac{J_z}{\Gamma} & \Gamma_8 = \frac{\left(J_x - J_y\right)J_x + J_{xz}^2}{\Gamma} \\ \Gamma_4 = \frac{J_{xz}}{\Gamma} & \Gamma_9 = \frac{J_x}{\Gamma} \\ \Gamma_5 = \frac{J_z - J_x}{J_y} & \Gamma = J_x J_z - J_{xz}^2 \\ V_a^b = \begin{bmatrix} u - u_w \\ v - v_w, \\ w - w_w \end{bmatrix} & V_a = ||V_a^b|| \end{cases}$$

3.1.3 External forces and moments

The external forces can be divided in three main factors, namely gravitational, aerodynamic and propeller forces. The gravitational force is expressed in the body frame as in (6).

$$F_g^b = \begin{pmatrix} -Mg\sin\theta \\ Mg\cos\theta\sin\phi \\ Mg\cos\theta\cos\phi \end{pmatrix} \tag{6}$$

The aerodynamic forces are expressed as a function of the airspeed relative to the plane (V_a defined above) and several aerodynamic coefficients which depend on the shape of the foils as well as the attitude of the body with respect to the air flow. These forces act on the three directions of the aircraft frame: they oppose the forward movement towards north with F_{drag}, they hold the plane up on the sky with F_{lift} and they displace the plane laterally with F_y. Usually, the aerodynamic forces and moments are decomposed in two groups: the longitudinal one with pitch moment (m in (5)) and its mechanical efforts expressed in (7), and the lateral one with its roll and yaw moments (l and n in (5)) and its effort in (8).

$$\begin{aligned} F_{lift} &= \frac{1}{2}\rho V_a^2 SC_L(\alpha, q, \delta_e) \\ F_{drag} &= \frac{1}{2}\rho V_a^2 SC_D(\alpha, q, \delta_e) \end{aligned} \tag{7}$$

$$F_y = \frac{1}{2}\rho V_a^2 SC_Y(\beta, p, r, \delta_a, \delta_r) \tag{8}$$

Finally, the thrust force produced by the propeller depends on the motor used and the speed of the plane through the air. It is not detailed here as the aircraft is only used in glider mode throughout the experiments.

The linearized relationship between aileron displacement δ_a and roll angle ϕ is obtained in the following. Developing (2), we find that $\dot{\phi} = p + q\sin\phi\tan\theta + r\cos\phi\tan\theta$. Considering

$$C_l = C_{l_0} + C_{l_\beta}\beta + C_{l_p}\frac{b}{2V_a}p + C_{l_r}\frac{b}{2V_a}r + C_{l_{\delta_a}}\delta_a + C_{l_{\delta_r}}\delta_r,$$

$$C_n = C_{n_0} + C_{n_\beta}\beta + C_{n_p}\frac{b}{2V_a}p + C_{n_r}\frac{b}{2V_a}r + C_{n_{\delta_a}}\delta_a + C_{n_{\delta_r}}\delta_r,$$

$\theta \approx 0$ and the effects of pitch and yaw rates (q, r) to be negligible over $\dot{\phi}$, we derive this equation with respect to time and substitute the expression of $\dot{p}$ given in (4). Because of the moments l and n, the aileron deflection δ_a appears. The coefficients C_{l_0} and C_{n_0} are null for symmetric aircrafts and the sideslip angle is taken as $\beta \approx 0$ to obtain the following transfer function:

$$\frac{\phi(s)}{\delta_a(s)} = \frac{a_{\phi_2}}{s(s + a_{\phi_1})} \tag{9}$$

where s is the Laplace operator, $a_{\phi_2} = 1/2\rho V_a^2 SbC_{p_{\delta_a}}$, $a_{\phi_1} = 1/4\rho V_a Sb^2 C_{p_p}$, $C_{p_{\delta_a}} = \Gamma_3 C_{l_{\delta_a}} + \Gamma_4 C_{n_{\delta_a}}$ and $C_{p_p} = \Gamma_3 C_{l_p} + \Gamma_4 C_{n_p}$.

3.2 Model identification procedure

3.2.1 State of the art

Flying tests are a cheap way to evaluate the aerodynamics of a plane. The classical method used for the determination of aerodynamic coefficients, or aerodynamic derivatives, is the testing in wind tunnels [11, 4]. It has been used to design the airfoil of the plane and so, to determine aerodynamic coefficients with satisfactory results. However, this approach requires a wind tunnel big enough to at least a plane wing to fit in the best case scenario. Other solutions are to use some simulation tools to deduce the aerodynamic coefficients. Some of them are freely available, such as XFoil and XFLR5[4]. It can be a good start to create a model of the plane, evaluate stability properties and obtain aerodynamic coefficients.

Other works have dealt with the determination of the aerodynamic coefficients through flight tests, such as [12, 13, 14, 15]. Many articles do not have or do not detail a proper flight protocol to obtain the sought aerodynamic coefficients, but some of them do. We find, for instance, methods that extract information from the phugoid mode [4], as well as from the dutch-roll mode[5]. Some other works generate a specific input excitation signal to the control surfaces in order to identify the plane model. The works [5, 16] propose the use of frequency sweep with a rich enough range of frequencies to obtain good estimates of the aerodynamic derivatives.

Furthermore, in order to get a good evaluation of the aerodynamic coefficients as a function of the angle of attack, a proposed method is to let the plane descend with a constant speed and several different slopes to get the aerodynamic coefficients for different angles of attack, either gliding or with activated thrusters. Paper [17] proposes positive and negative slopes for the test. Likewise, [18] presents an identification technique with data obtained from a straight and level path at a constant throttle setting over a large distance. Particularly for our plane, it was not possible to measure the airspeed and activate the thruster at the same time due to the location of the Pitot probe in the wake of the propeller. Therefore, we performed experiments in glide configuration because the activation of the thruster creates a perturbation flow which distorts the sensor's measurements.

Finally, other methods for determining aerodynamic derivatives can be based on neural networks, like in [19]. However, a massive amount of training data is required for a precise identification and a re-initialization for every new type of aircraft model must be performed as well.

In the sequel, we propose two new (in-flight and out-flight) aircraft model identification techniques.

[4] https://sourceforge.net/projects/xflr5/

[5] http://www.xflr5.tech/docs/XFLR5_Mode_Measurements.pdf

3.2.2 In-flight data identification

For the in-flight data identification procedure, data is collected during the flight and used for identifying a transfer function. This strategy has been chosen in several different papers, some of them employing circular and ascending or descending trajectories [20, 17] and others, producing a sinusoidal input of varying frequency [16, 5]. On the one hand, the use of circular and ascending or descending trajectories may have poor frequency content. On the other hand, the use of frequency-varying sinusoidal inputs requires either changing the radio controller firmware[6] or modifying the autopilot firmware. Concerning the autopilot firmware modification, a more user-friendly approach is to use the Matlab Embedded Coder Support Package for PX4 Autopilots[7]. Summarizing, the so-far presented options can be either financially or technically costly, depending on the user. We have chosen to explore an approach where the pilot maneuvers the plane in an arbitrary design that fairly excites the different modes of the airplane.

The analysis here introduced consists in the characterization of the dynamic relationship between aileron deflection and roll movement by means of a transfer function, but the technique can be transposed for the identification of other relations, eg. elevator deflection to pitch angle and rudder deflection to yaw angle.

Note that, because of the mathematical development that leads to (9), we seek a transfer function of degree 2. Furthermore, through the current method we are interested in identifying the unknown parameters $a_{\phi 1}$ and $a_{\phi 2}$. These parameters are dependent upon aerodynamic coefficients, airspeed, air density, coefficients of inertia and aircraft dimensions, therefore the knowledge of $a_{\phi 1}$ and $a_{\phi 2}$ can lead to the identification of the unknown aerodynamic coefficients. This latter identification was not performed in the scope of this work, but would certainly be a pertinent investigation.

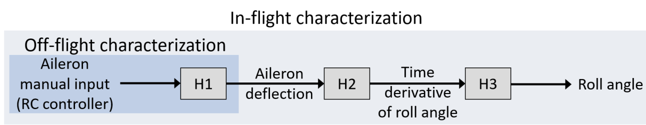

Figure 2: Identification of the transfer function (manual aileron inputs to roll angle). Image modified from [21].

Figure 2 presents how an aileron input affects the roll angle. The relationship between aileron deflection and aileron manual inputs (i.e. H1) is characterized off-flight, by measuring with an incidence meter the aileron displacements associated to various manual aileron inputs (*cf.* Figure 3). This procedure disregards any existing dynamics between manual aileron inputs and aileron displacements under the hypothesis that the aileron dynamics is much faster than the aircraft dy-

[6] https://www.open-tx.org/lua-instructions.html

[7] https://fr.mathworks.com/matlabcentral/fileexchange/70016-embedded-coder-support-package-for-px4-autopilots

namics. From Figure 3, we find that the block H1 can be approximated by a constant gain of value 0.0466. Once H1 has been determined, the transfer function H2·H3 is yet to be obtained. This is done with flight tests, from which H1 ·H2·H3 can be identified. Furthermore, from the transfer function (9), we know that the block H3 consists of an integrator.

In the flight test, we bring the airplane up to a certain altitude and, then, we excite the ailerons arbitrarily in amplitude and frequency while the airplane is in glider mode, having its throttle input at zero. Such an aileron input signal is convenient for being easily produced and for allowing rich excitation due to the fast variations of the joystick. To illustrate it, two realizations of aileron manual input signals are shown in Figure 4.

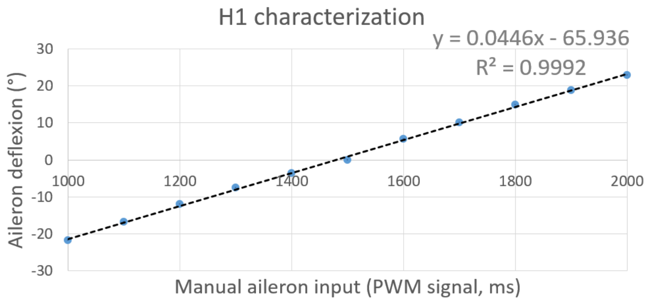

Figure 3: Characterization of the relation (manual aileron inputs to roll angle) through linear regression over the measurements. Image modified from [21].

Once the experiment is performed, a file of format *.ulg* containing several recorded measurements is produced. Two visualization tools available for interpreting these files are Flight Review[8] and pyulog[9]. Particularly with the latter one, it is possible to obtain *.csv* files that can be read by general-purpose applications, such as Matlab and Octave. There also exists a parser, named plotulog[10] that uses pyulog and Octave to display the measurements contained in a *.ulg* file. In a *.ulg* file, one can find information about the plane's altitude, attitude, airspeed, manual control inputs, actuator outputs, GPS position, battery voltage, and more. For our study, we use altitude, thruster, roll and aileron manual inputs to select the experiment windows and to identify transfer functions.

Experiments were performed in glider configuration, meaning that the throttle input was null over the test interval. This is particularly important for our case because of the Pitot probe placement in the wake of the propeller, *cf.* Figure 5. The test datasets were, therefore, taken from the time intervals in which the altitude had an overall decreasing slope and throttle was deactivated, as shown in Figure 6. In this particular dataset, the experiments done by exciting the aileron manual inputs are given by the second, third and fifth grey areas.

[8]`https://docs.px4.io/en/log/flight_review.html`
[9]`https://github.com/PX4/pyulog`
[10]`https://github.com/kyuhyong/plotulog`

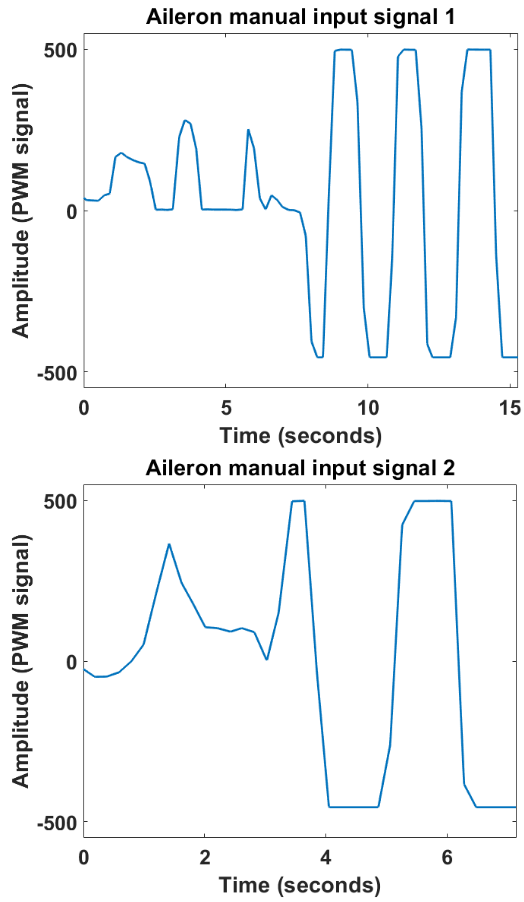

Figure 4: Realizations of arbitrary aileron manual input signals.

Manual inputs, as well as other data, may contain biases. For our experiments, we must observe whether the aileron manual input data contains a bias and, if so, remove it, so that the system identification algorithms can work properly. Furthermore, we know that the transfer function between aileron displacement and roll angle is of second order and that one of its poles is an integrator. Because the integrator is an unstable pole, in the first moment, we identify the transfer function between the aileron manual input and the time derivative of the roll angle. The roll angle is a discrete vector, and its discrete derivative was computed using backward differences divided by the sampling time.

Once the data intervals are selected, system identification can be performed. In our case, we used the Matlab system identification toolbox while calling the functions *data = iddata(OutputVector,InputVector,SamplingTime,'Tstart',0)* to define input-output data objects from excerpts of the flight data; *tf_data = tfest(data,1,0)*[11] to estimate a transfer function from *data* containing 1 pole and no zeros; and *fit = compare(data,tf_data)* to ascertain how good the estimated trans-

[11]The function *tfest* initializes the sought parameters with the Instrument Variable method and obtains its estimation by the minimization the weighted prediction error norm.
Source: `https://fr.mathworks.com/help/ident/ref/tfest.html`

Figure 5: Plane with highlighted propeller and Pitot probe.

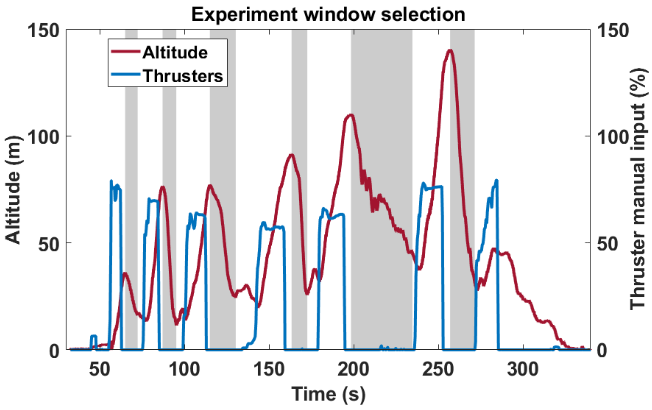

Figure 6: Selection of time intervals for the time experiments indicated by grey areas.

fer function is to reproduce the input-output behavior stored in the object *data*. The quantity *fit* is the "normalized root mean square (NRMSE) measure of the goodness of the fit between simulated response and measurement data"[12].

Besides the Matlab toolbox, there are several other open source alternatives to perform system identification, such as Mataveid[13], Octave system identification toolbox[14], SIPPY[15] or Contsid[16].

For approximate airspeeds, each experiment can be used as training dataset for a transfer function and can be validated using all the datasets. In this sense, for $\mathbf{n}$ datasets, $\mathbf{n}$ transfer functions can be produced, and we can calculate $\mathbf{n}$ values of fit for each transfer function. Among the $\mathbf{n}$ identified transfer functions, we must choose the most suitable to represent the system dynamics in the time derivative of the roll. For that, we perform a weighted average of the fit values produced by each transfer function. Given that the manual aileron inputs in the radio controller are arbitrary, we can imagine that some sequences have better quality than others, being able to produce a transfer function that better represents the overall behavior of the aircraft on the roll axis. These "good quality experiments" have better fit coefficients for most of the transfer functions, so we can consider that they might give more reliable information on the identification process. We consider an experiment to be of *acceptable quality* if the sum of its $\mathbf{n}$ fits is positive. Therefore, we can expect that $\mathbf{q}$ experiments are of acceptable quality, $\mathbf{q} \leq \mathbf{n}$. For example, in Table 3 $\mathbf{n} = \mathbf{q} = 3$, while in Table 7, $\mathbf{n} = 10$ and $\mathbf{q} = 9$.

tf \ ex	1	2	3
1	79.9296	74.7091	82.3494
2	78.7124	75.8576	82.0165
3	79.6587	75.3255	82.6885
sum	238.3008	225.8921	247.0544

Table 3: Values of fit for each transfer function and each experiment (aileron displacement to time derivative of roll angle).

Therefore, the calculation of a general fit for a transfer function obtained from a given dataset is given as:

$$F_{d,i,\mathbf{q}} = \frac{\sum_{j=1}^{\mathbf{q}} f_{d,i,j} \sum_{k=1}^{\mathbf{n}} f_{d,k,j}}{\sum_{l=1}^{\mathbf{n}} \sum_{m=1}^{\mathbf{q}} f_{d,l,m}} \tag{10}$$

where $F_{d,i,\mathbf{q}}$ stands for the general fit of the i-th transfer function from the dataset d and $f_{d,i,j}$ is the fit of i-th transfer function using j-th experiment as validation data. The general fit values obtained from the time derivative of the roll angle are indicated as $F_{\dot{\phi},i,\mathbf{q}}$, with $i = 1, \ldots, \mathbf{n}$, see Table 4.

tf	1 $\frac{51.48}{s+17.05}$	2 $\frac{58.04}{s+18.35}$	3 $\frac{53.2}{s+16.32}$
$F_{\dot{\phi},i,3}$	79.1121	78.9534	79.3349

Table 4: General fit values obtained from the derivative of the roll angle.

Afterwards, we add an integrator to the found transfer functions and proceed with the fit calculation on roll angle data. We expect that, out of the $\mathbf{n}$ data intervals, $\mathbf{r}$ are of acceptable quality, $\mathbf{r} \leq \mathbf{n}$. Likewise, we can come up with a weighted average of the fit values produced by each transfer function and calculate a general fit as in (10), that we identify with $d = \phi$. These general fit values are, therefore, represented as $F_{\phi,i,\mathbf{r}}$, with $i = 1, \ldots, \mathbf{n}$. At this point, we have two general fit values associated to each transfer function: one related to the roll angle, and the other to its time derivative. To choose the best transfer function candidate, we perform a

[12] `https://fr.mathworks.com/help/ident/ref/compare.html`
[13] `https://github.com/DanielMartensson/Mataveid`
[14] `https://octave.sourceforge.io/control/overview.html`
[15] `https://github.com/CPCLAB-UNIPI/SIPPY/blob/master/user_guide.pdf`
[16] `http://www.contsid.cran.univ-lorraine.fr/`

weighted average given by:

$$\mathcal{F}_i = \frac{\left(\sum_{l=1}^{\mathbf{n}}\sum_{m=1}^{\mathbf{q}} f_{\dot{\phi},l,m}\right)\cdot F_{\dot{\phi},i,\mathbf{q}} + \left(\sum_{l=1}^{\mathbf{n}}\sum_{m=1}^{\mathbf{r}} f_{\phi,l,m}\right)\cdot F_{\phi,i,\mathbf{r}}}{\left(\sum_{l=1}^{\mathbf{n}}\sum_{m=1}^{\mathbf{q}} f_{\dot{\phi},l,m}\right) + \left(\sum_{l=1}^{\mathbf{n}}\sum_{m=1}^{\mathbf{r}} f_{\phi,l,m}\right)} \tag{11}$$

Finally, the function with highest value $\mathcal{F}_i$ is the best suitable transfer function to represent the relation between aileron deflection and roll angle. Recalling Figure 3, to obtain the transfer function from aileron displacement to roll angle, we must multiply each transfer function by $1/\text{H1}$. For this experiment, results are found in Table 5. A comparison between the expected input-output behavior and the outcome from the identified transfer functions can be found in Figure 7. Some of the reasons that contribute to the disparity between the expected validation curve and the transfer functions' outcomes are the numerous simplifications that convert the full airplane nonlinear system into a linear one, the disregard of wind inflow and inter-axes couplings, and the consideration that every experiment was performed under constant airspeed.

tf	1	2	3
	$\frac{51.48}{s^2+17.05s}$	$\frac{58.04}{s^2+18.35s}$	$\frac{53.2}{s^2+16.32s}$
$\mathcal{F}_i$	77.62	79.53	78.73
airspeed (m/s)	22.22	26.67	31.17

Table 5: Aileron displacement to roll angle identified transfer functions.

To confirm the aforementioned findings, results for data of a second flight, similar to the previous one and containing 10 experiments, can be found in Appendix A.

3.2.3 Out-flight data identification

XFLR5 is an open-source program that performs foil analysis and 3D analysis for aircraft using a combination of inviscid vortex-lattice method and viscous analysis. With this application, we can import and modify foils, create a plane model, generate polar curves for different Reynolds numbers, evaluate efforts for different angles of attack, compute stability properties and aerodynamic derivatives, visualize the movement caused by airplane dynamic modes, and so on. In this section, we use the software XFLR5 to calculate the aerodynamic coefficients of the aircraft. We do so by building a model of the airplane in XFLR5 (*cf.* Figure 8) and equipping it with ailerons.

We ascertain whether the plane is pitching moment inherently stable by performing a *Plane analysis* and verifying that the pitching moment (Cm) is a negative-slope function of the angle of attack. Then, we perform a stability analysis with

[17] https://youtu.be/U7sa0cozpi8

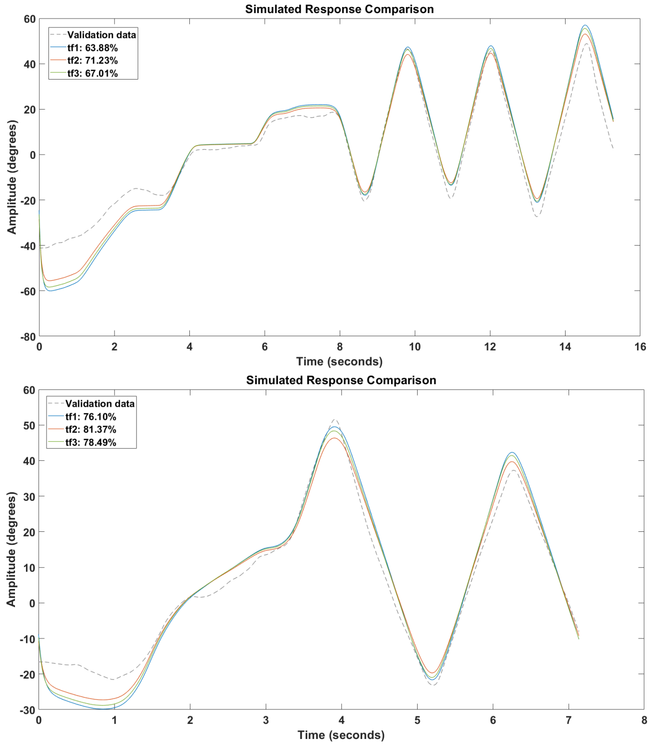

Figure 7: Comparison between the expected input-output behavior (Validation data) and the outcome from the identified transfer functions (tf1, tf2, tf3).

actuated ailerons. The analysis is recorded in a log file that provides various information about inertia coefficients, lateral and longitudinal modes, and aerodynamic coefficients. We can use this data to either complete a full nonlinear model of the plane, or to compose an already linearized dyamic model to compute a transfer function. In the first case, in [8] it is suggested to use Matlab and Simulink for building the nonlinear model, numerically "trimming" it to a specific trajectory and computing the associated transfer functions. In the second case, one can use open source tools, such as Octave[18] or Python language[19], to define a transfer function and evaluate its properties.

$\mathbf{V_a}$	11.46m/s	$\mathbf{S}$	0.637m^2
$\mathbf{b}$	3.18m	$\mathbf{J_x}$	0.869kg/m^2
$\mathbf{J_z}$	1.093kg/m^2	$\mathbf{J_{xz}}$	-0.003446kg/m^2
$\mathbf{C_{l_{\delta_a}}}$	0.3381	$\mathbf{C_{n_{\delta_a}}}$	0.00005847
$\mathbf{C_{l_p}}$	-0.6440	$\mathbf{C_{n_p}}$	-0.07775

Table 6: XFLR5 stability analysis coefficients for our plane model and $\rho = 1.225\text{kg/m}^3$.

The transfer function associated to the aileron deflection

[18] https://octave.sourceforge.io/control/function/tf.html

[19] https://python-control.readthedocs.io/en/latest/classes.html

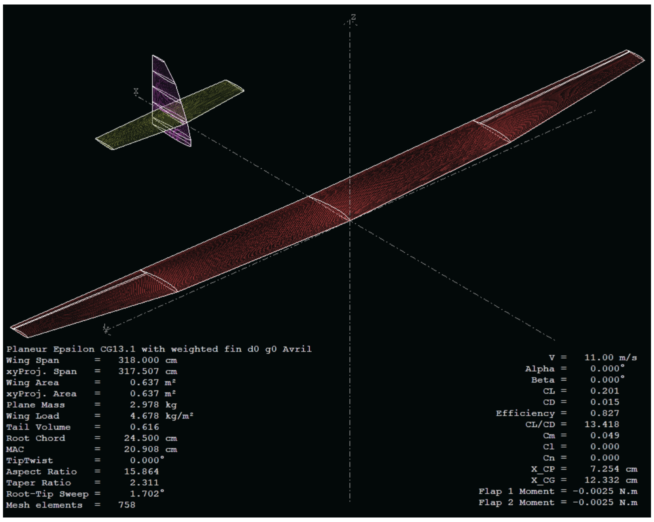

Figure 8: XFLR5 plane model. Note that the model does not contain the body of the plane. This is a recommended practice to avoid numerical issues[17].

and roll angle is given in (9). Among the terms that compose this transfer function, ρ is given by the user, and V_a, S, b, J_x, J_z, J_{xz}, $C_{l_{\delta_a}}$, $C_{n_{\delta_a}}$, C_{l_p} and C_{n_p} are calculated by the XFLR5 stability analysis. The airspeed V_a given by the analysis is the speed that balances the airplane weight. From the stability analysis ran in the airplane model, we obtain the coefficients in Table 6, leading to the resulting transfer function:

$$\frac{\phi(s)}{\delta_a(s)}_{XFLR5} = \frac{63.40}{s(s+16.75)}. \tag{12}$$

We notice that this transfer function presents a gain and poles that are close to the ones found for in-flight experiments with approximate airspeed (*cf.* Appendix A, Table 11, tf9). As a matter of fact, for a difference of airspeeds of $|\Delta V_a| = 0,41365$m/s, we observe a difference between the gains of 1.2801, or 2% with respect to tf9 gain, and a difference between the poles of 1.8482, or 10% with respect to the tf9 non-null pole. However, note that the same does not happen for different airspeeds. For instance, for an airspeed $V_a = 22.2235$m/s, we obtain $\frac{\phi(s)}{\delta_a(s)}_{XFLR5} = \frac{238.49}{s(s+32.49)}$, a very different result from what was obtained in Table 5.

3.2.4 Comparison of in-flight and out-flight identification methods

We stress the fact that both in-flight and off-flight identification techniques are subject to different types of approximations and have advantages and pitfalls. In the in-flight case, we can perform relatively simple experiments and use largely known identification techniques to compute a transfer function. These functions are obtained with the simplifying hypotheses that inter-axes couplings and influences of the wind are negligible, and that the airspeed is constant. On the other hand, the current out-flight identification technique does not even require flight data and can be done by directly calculating the coefficients of (9). However, this technique is also subject to simplifications associated to neglecting inter-axes couplings and the airplane body in the aerodynamic coefficients' calculations. Furthermore, the author of XFLR5 warns that "XFLR5 postulates that the viscous and inviscid contributions to aerodynamic forces are linearly independent" and that "the independence hypothesis is not supported by a theoretical model" [22].

4 CONCLUSIONS AND PERSPECTIVES

In this article we present two different methodologies for airplane model identification that rely on opensource solutions, we propose a flight protocol of simple execution and we bring together some of the state of the art techniques in airplane model identification. Experiments are performed in order to characterize the relationship between aileron deflection and roll angle. One of the air plane model identification methods requires in-flight data and uses the suggested flight protocol. The other utilizes aerodynamic coefficients obtained from a virtual plane model. For the same airspeeds, both techniques convey results in the same order of magnitude. This work aimed to determine a standard protocol for parameter identification through a set of procedures, preferably simple, that leads to an accurate modeling of aircraft input-output behavior. The use of two independent techniques, in-flight and off-flight, endorse the accuracy of the found transfer functions.

As future work, we will evaluate these identification techniques with other planes, one of them being a flying wing, and proceed with the identification with other control surfaces. Knowledge about the dynamical behavior of different aircraft will integrate a Matlab model along with the PX4 PI-FF control structure, so that we will be able to simulate and tune the controller gains for each plane.

ACKNOWLEDGEMENTS

The ELCOD[20] project is co-funded by the European Regional Development Fund (ERDF) and the co-financed project partners Region Grand Est and the countries of Baden-Württemberg and Rhineland-Palatinate in the framework of the INTERREG V Upper Rhine program.

REFERENCES

[1] Emmanuel Roussel. *Contribution à la modélisation, l'identification et la commande d'un hélicoptère miniature*. PhD thesis, 2017.

[2] Robert F. Stengel. *Flight Dynamics*. Princeton University Press, 2004.

[3] Robert C. Nelson. *Flight Stability and Automatic Control*. McGraw-Hill Education, oct 1997.

[20] www.elcod.eu

[4] M. Scherer and P. Mathé. Mesure des derivées aérodynamiques en soufflerie et en vol. Technical report, Organisation du Traité de l'Atlantique Nord, 1961.

[5] Said S Hamada. *Development of a Small Unmanned Aerial Vehicle Longitudinal Model for Future Flutter Testing*. Master thesis, Embry-Riddle Aeronautical University, 2018.

[6] Lorenz Meier, Dominik Honegger, and Marc Pollefeys. PX4: A node-based multithreaded open source robotics framework for deeply embedded platforms. In *Proceedings of IEEE ICRA*, pages 6235–6240, jun 2015.

[7] E H J Pallett, Amraes S Coyle, and Msetp Blackwell. *Automatic Flight Control*. Wiley-Blackwell - 4th edition, dec 1993.

[8] Randal W. Beard and Timothy W. McLain. *Small Unmanned Aircraft*. Princeton University Press, apr 2015.

[9] Néstor Alonso Santos Ortiz. *Analyse de la robustesse de la loi de commande d'un quadrirotor embarquant une charge suspendue par câble*. Master iriv, INSA de Strasbourg, 2017.

[10] Bernard Etkin and Lloyd Duff Reid. *Dynamics of Flight: Stability and Control*. Wiley, oct 1995.

[11] *Modeling the Aircraft*, chapter 2, pages 63–141. John Wiley & Sons, Ltd, 2015.

[12] G. T. Chapman and D. B. Kirk. A method for extracting aerodynamic coefficients from free-flight data. *AIAA Journal*, 8(4):753–758, 1970.

[13] Lawrence E. Hale, Mayuresh Patil, and Christopher J Roy. Aerodynamic Parameter Identification and Uncertainty Quantification for Small Unmanned Aircraft. *Journal of Guidance, Control, and Dynamics*, 40(3):680–691, 2016.

[14] Jieliang Shen, Yan Su, Qing Liang, and Xinhua Zhu. Calculation and identification of the aerodynamic parameters for small-scaled fixed-wing UAVs. *Sensors (Switzerland)*, 18(1), jan 2018.

[15] Ruiyong Zhai, Zhaoying Zhou, Wendong Zhang, Shengbo Sang, and Pengwei Li. Control and navigation system for a fixed-wing unmanned aerial vehicle. *AIP Advances*, 4(3), mar 2014.

[16] Watcharapol Saengphet, Suradet Tantrairatn, Chalothorn Thumtae, and Jiraphon Srisertpol. Implementation of system identification and flight control system for UAV. In *Proceedings of 3rd IEEE ICCAR 2017*, pages 678–683, jun 2017.

[17] Brent Michalowski and Nathaniel Varano. UAV flight test characterization using minimal test equipment. *Proceedings of ICUAS 2017*, pages 1737–1741, 2017.

[18] Jon Ostler and W. Bowman. Flight Testing of Small, Electric Powered Unmanned Aerial Vehicles. *2005 U.S. Air Force T&E Days*, 1(3), 2005.

[19] Dennis J. Linse and Robert F. Stengel. Identification of aerodynamic coefficients using computational neural networks. *Journal of Guidance, Control, and Dynamics*, 16(6):1018–1025, 1993.

[20] Pedro L. Jimenez, Jorge A. Silva, and Juan S. Hernandez. Experimental validation of Unmanned Aerial Vehicles to tune PID controllers in open source autopilots. *Proceedings of the 7th EUCASS*, 2017.

[21] Anthony Coindevel and Eustáquio Fernandes. Commande de drone de type Avion dans le cadre du projet ELCOD - Rapport final - Projet de Recherche Technologique, INSA Strasbourg. Technical report, 2017.

[22] Model analysis with XFLR5. In *R/C Soaring Digest 2008*.

Appendix A Data from a second in-flight experiment

tf \ ex	1	2	3	4	5
1	66.77	25.51	12.88	-50.26	70.11
2	41.59	35.92	16.82	-41.26	57.58
3	45.08	35.34	16.96	-42.93	60.12
4	-9.62	-29.46	5.71	3.93	-9.54
5	63.36	24.29	13.64	-51.84	73.80
6	64.67	22.90	12.62	-52.16	72.69
7	63.91	27.96	14.85	-49.84	73.09
8	58.15	30.96	16.00	-47.91	69.13
9	63.77	24.43	13.62	-51.73	73.77
10	61.15	20.94	12.47	-53.47	73.33
sum	518.82	218.79	135.57	-437.46	614.08

tf \ ex	6	7	8	9	10
1	46.51	70.66	59.93	73.43	74.07
2	38.86	60.44	59.17	58.79	57.14
3	40.01	63.23	62.20	61.82	60.49
4	-0.97	-3.10	-6.44	-4.66	-2.18
5	46.59	72.28	62.32	75.70	77.31
6	46.96	71.17	59.79	75.15	76.94
7	46.22	73.05	64.61	74.99	75.42
8	44.14	70.96	66.49	71.27	71.07
9	46.68	72.31	62.21	75.71	77.25
10	46.53	70.60	59.67	75.15	77.81
sum	401.54	621.58	549.95	637.36	645.32

Table 7: Values of fit for each transfer function and each experiment (aileron displacement - time derivative of roll angle). The columns in black color contain experiments of acceptable quality.

tf	1	2	3	4
	$\frac{23.68}{s+161.9}$	$\frac{1.598}{s+15.61}$	$\frac{1.269}{s+11.41}$	$\frac{-0.03452}{s+6.141e-05}$
$F_{\dot{\phi},i,9}$	63.3592	52.2972	54.8808	-6.1620
tf	5	6	7	8
	$\frac{2.732}{s+17.55}$	$\frac{4.439}{s+28.35}$	$\frac{2.517}{s+17.25}$	$\frac{1.552}{s+11.37}$
$F_{\dot{\phi},i,9}$	64.7947	64.1104	64.9631	62.4581
tf	9	10		
	$\frac{2.885}{s+18.6}$	$\frac{2.93}{s+17.91}$		
$F_{\dot{\phi},i,9}$	64.8382	63.6704		

Table 8: General fit values obtained from the derivative of the roll angle.

tf \ ex	1	2	3	4	5
1	95.54	-112.19	-167.79	-56.05	-127.79
2	64.80	-40.21	-103.34	-37.89	-60.41
3	68.47	-51.15	-115.93	-40.59	-73.29
4	65.90	-70.51	34.93	86.89	-344.35
5	93.52	-123.80	-181.93	-58.53	-142.94
6	95.20	-126.98	-183.58	-59.50	-144.37
7	89.73	-107.92	-167.18	-54.75	-127.24
8	81.93	-90.33	-152.85	-50.23	-112.27
9	93.69	-123.06	-181.04	-58.39	-141.94
10	93.49	-136.76	-193.92	-61.59	-155.73
sum	842.3	-982.9	-1412.6	-390.6	-1430.4

tf \ ex	6	7	8	9	10
1	4.88	-34.98	61.23	-32.70	5.90
2	8.97	-11.55	63.55	2.01	20.14
3	8.52	-15.59	67.16	-4.13	17.92
4	29.45	-43.87	-3.58	-78.06	-39.60
5	3.34	-40.45	61.43	-41.43	1.38
6	3.18	-41.17	59.62	-42.21	1.03
7	4.86	-34.48	65.01	-32.49	5.96
8	6.13	-28.88	68.84	-24.30	9.63
9	3.44	-40.09	61.48	-40.84	1.71
10	1.97	-45.44	57.81	-48.84	-2.59
sum	74.7	-336.5	562.6	-343.0	21.5

Table 9: Values of fit for each transfer function and each experiment (aileron displacement - roll angle). The columns in black color contain experiments of acceptable quality.

tf	1	2	3	4
	$\frac{23.68}{s(s+161.9)}$	$\frac{1.598}{s(s+15.61)}$	$\frac{1.269}{s(s+11.41)}$	$\frac{-0.03452}{s(s+6.141e-05)}$
$F_{\phi,i},4$	76.8858	60.9124	64.2674	36.5376
tf	5	6	7	8
	$\frac{2.732}{s(s+17.55)}$	$\frac{4.439}{s(s+28.35)}$	$\frac{2.517}{s(s+17.25)}$	$\frac{1.552}{s(s+11.37)}$
$F_{\phi,i},4$	75.6831	75.9327	75.0408	72.2169
tf	9	10		
	$\frac{2.885}{s(s+18.6)}$	$\frac{2.93}{s(s+17.91)}$		
$F_{\phi,i},4$	75.8080	74.1839		

Table 10: General fit values obtained from the roll angle.

tf	1	2	3	4
	$\frac{530.9}{s(s+161.9)}$	$\frac{35.83}{s(s+15.61)}$	$\frac{28.45}{s(s+11.41)}$	$\frac{-0.7739}{s(s+6.141e-05)}$
$\mathcal{F}_i$	66.8336	54.5100	57.2918	4.8055
V_a (m/s)	11.1412	8.7697	13.2818	13.7666
tf	5	6	7	8
	$\frac{61.25}{s(s+17.55)}$	$\frac{99.52}{s(s+28.35)}$	$\frac{56.44}{s(s+17.25)}$	$\frac{34.79}{s(s+11.37)}$
$\mathcal{F}_i$	67.5914	67.1470	67.5516	64.9647
V_a (m/s)	11.1168	11.5762	10.7339	9.7307
tf	9	10		
	$\frac{64.68}{s(s+18.6)}$	$\frac{65.69}{s(s+17.91)}$		
$\mathcal{F}_i$	67.6558	66.3708		
V_a (m/s)	11.0446	12.0568		

Table 11: Aileron displacement - roll angle identified transfer functions.